Atmos. Meas. Tech. Discuss., https://doi.org/10.5194/amt-2017-318
Manuscript under review for journal Atmos. Meas. Tech.
Discussion started: 3 November 2017

Atmospheric Measurement Techniques Discussions
Open Access
EGU

Comparison of aerosol optical depth from satellite (MODIS), Sun photometer and pyrheliometer ground-based measurements in Cuba.

Juan Carlos Antuña-Marrero[1], Victoria Cachorro Revilla[2], Frank García Parrado[1], Ángel de Frutos Baraja[2], Albeth Rodríguez Vega[1], David Mateos[2], René Estevan Arredondo[3,1], Carlos Toledano[2]

[1] Atmospheric Optics Group of Camagüey (GOAC), Meteorological Institute of Cuba, Camagüey, Cuba
[2] Atmospheric Optics Group (GOA), University of Valladolid (UVA), Valladolid, Spain
[3] Huancayo Observatory, Geophysical Institute of Peru, Huancayo, Peru

Corresponding author:
Juan Carlos Antuña-Marrero
Atmospheric Optics Group of Camagüey
Meteorological Institute of Cuba
Camagüey, Cuba
Email: jcam45@gmail.com

Atmos. Meas. Tech. Discuss., https://doi.org/10.5194/amt-2017-318
Manuscript under review for journal Atmos. Meas. Tech.
Discussion started: 3 November 2017

Atmospheric Measurement Techniques Discussions

Abstract:

In the present study, we report the first comparison of the aerosol properties measured with sun photometer at Camagüey, Cuba, with the MODerate resolution Imaging Spectroradiometer (MODIS) instruments on Terra and Aqua satellites. We compared the aerosol optical depth at 550 nm (AOD) and the Ångström Exponent (AE) from the sun photometer for the period 2008 to 2014 with the same variables measured by both MODIS instruments, that are spatially and temporally coincident. The comparison includes AOD derived with both Deep Blue (DB) and Dark Target (DT) algorithms from MODIS Collection 6. The AOD derived with DT algorithm for Terra and Aqua agrees better with AOD from the sun photometer than the AOD derived with DB. Additionally there is little difference between AOD from both satellite instruments, when they are compared with sun photometer AOD, allowing to combine AOD from Terra and Aqua for more comprehensive climatological statistics. The comparison of the AE showed similar results with reports in the literature about the little skills of the current DT and DB algorithms for its retrieval. In addition, we report the comparison of the broadband AOD (BAOD) from pyrheliometer measurements located at Camagüey site and other three meteorological stations along Cuba, with AOD measurements from the sun photometer and from MODIS onboard Terra and Aqua. The comparison of the BAOD from the four sites as a whole with coincident AOD from MODIS onboard Terra and Aqua showed similar results than the ones of the comparison between the sun photometer AOD and the AOD from the two satellite instruments. In the comparison between the BAOD and the AOD at each one of the eight individual sun photometer wavelengths, the results improve in the spectral range 400 to 675 nm, with the best result at 500 nm. The BAOD typical uncertainty ranges from 0.04 to 0.06 at this band. The results from the BAOD comparisons demonstrate its reliability for characterizing AOD at sites with no sun photometer and for extending backward in time AOD estimates.

KEY WORDS: Atmosphere, Remote sensing, Aerosols, Aerosol optical depth (AOD), Broadband Aerosol optical depth (BAOD), AERONET, MODIS

1. Introduction:

Although atmospheric aerosols have a small mass, they play an important role in weather and climate. Depending on the physical and chemical properties of the aerosol, its origin and its spatial and temporal distribution they affect radiative transfer, dynamic, biogeochemical and chemical Earth's processes (Knippertz and Stuut, 2014; Seinfeld and Pandis, 2016). Atmospheric aerosols have a strong effect on the atmospheric latent heating spatial heterogeneity and the atmospheric radiative transfer (IPCC, 2013). Aerosols can also affect the biosphere and, in particular, humans in several ways. For example, in the case of the Saharan dust transported to America across the Atlantic, it supplies nutrients to the Amazon forest (Swap et al., 1992; Yu et al., 2015). Moreover, in the Caribbean, in addition to the locally originated aerosols, dust makes the aerosol amount to exceed the air quality standards associated to human health effects (Prospero and Lamb, 2003; Prospero et al., 2014). The great variability of Saharan dust transported to the Caribbean basin has been documented using long-term measurements in Barbados (Prospero and Lamb, 2003; Prospero and Mayol-Bracero, 2013) and more recently measurements in Miami, Guadeloupe and Cayenne (Prospero et al., 2014).

The earliest attempt to measure the aerosol optical properties in Cuba registered in a scientific publication, comes back to 1988. Using a Linke Feussner pyrheliometer, direct normal irradiance (DNI) measurements were conducted in Havana between 1977 and 1985.The Linke turbidity factor and the Ångström turbidity coefficient were calculated (Martinez, 1988). Results were limited because of the fact that the Linke turbidity factor represents the combined turbidity of aerosols, water vapor and NO_2, while the Ångström turbidity coefficient could only be determined if the Ångström Exponent is assumed a priori. Twenty years later a cooperation agreement between scientific institutions of Spain and Cuba, allowed the installation of a Cimel CE-318 sun photometer at Camagüey (Cuba) and its inclusion in the Aerosol Robotic Network (AERONET, Holben et al., 1998). Several studies have been conducted using the Aerosol Optical Depth (AOD) and AE observations from Camagüey's sun photometer (see, Antuña et al, 2016). Broadband Aerosol Optical Depth (BAOD) estimates complement sun photometer aerosol measurements at Camagüey but also provide aerosol information at other three locations in Cuba. The main purpose of BAOD is to provide information about the variability of aerosols along the island, making it also possible to extend the aerosol records back in time. Pyrheliometric DNI measurements allow the BAOD retrieval. The first BAOD calculations used for the DNI measurement were conducted at Camagüey under clear sky conditions for the period 1985-2007 using Gueymard's (1998) improved parameterizations (Fonte and Antuña, 2011). García et al. (2015)

made use of this kind of DNI measurements but for a longer period (1981-2013). They used observations under the clear line of sight between the pyrheliometer and a region of 5° around the Sun, as well as improved climatological values of the integrated water vapor.

In advance of the aerosol climatology for Cuba land areas, already under development, we have conducted a comparison of aerosol ground-based measurements and the available satellite data. It consists of the comparison among all available Camagüey's sun photometer AOD (500 nm) and AE, and the BAOD measurements at four Cuban locations, with the series of AOD (550 nm) and AE from the MODerate resolution Imaging Spectroradiometer (MODIS) instruments onboard Terra (2001 to 2015) and Aqua (2002 to 2015) satellites. Selected observations were the ones spatially and temporally collocated between the satellite instruments and the ground-based sites. One of the challenges we faced was the low amount of potential coincident AOD and AE from MODIS and Sun photometer. The same is true for AOD from MODIS and pyrheliometer BAOD, in both cases because of existing gaps in the ground-based time series. In order to maximize the number of satellite and surface measurement pairs, we used the primary AOD and AE L2 products without any averaging and the combined AOD and AE from Terra and Aqua MODIS sensors as a whole dataset.

Section 2 begins with the description of the datasets, followed by the explanation of the coincidence criteria between the MODIS AOD and AE L2 products and the same variables from the sun photometer, as well as the MODIS AOD L2 products and pyrheliometer BAOD. This section ends with the explanation of the statistics and the statistical methods used. Section 3 shows the results and discussion, followed by the summary and conclusions in section 4.

2. Materials and Methods:

2.1 *MODIS satellite instruments:*

The twin MODIS instruments onboard Terra and Aqua satellites accumulate more than 15 years of measurements of several atmospheric parameters, including AOD at several wavelengths and the AE, the two most common parameters to characterize the atmospheric aerosol optical properties. Depending on the assumptions about the properties of Earth's surface and the aerosol type expected over these surfaces, the MODIS Atmosphere team developed three algorithms for the processing of MODIS measurements (Levy et al., 2013). Regions visually "dark" from the space, named Dark Target (DT), include the algorithm assumptions for vegetated land surfaces (Kaufman et al., 1997) and for remote ocean regions (Tanré et al., 1997). The third algorithm, called Deep Blue (DB) algorithm, includes assumptions for surfaces visually "bright" from space and makes use of the near-UV (DB band near 410 nm).

Under these conditions, the DB band provides a better signal than the visible wavelengths, improving the signal for aerosol retrievals (Hsu et al., 2004; 2006) due to lower surface albedo at this short wavelength. Levy et al. (2013) provides a detailed explanation of MODIS basic retrieval concepts and the improvements of the DT algorithm in Collection 6 for aerosol products. In addition, Hsu et al. (2013) makes a detailed explanation of the DB algorithm improvements in Collection 6.

Following Levy et al. (2013) we summarize the MODIS calculus chain. MODIS Level 0 (L0) is the basic data file, containing the raw measurements from the sensors. Measurements grouped in 5 minutes swath scans (called granules) are Level 1A (L1A), which after calibration becomes Level 1B (L1B). L1B data feed the MODIS geophysical retrieval algorithms, generating the very primary geophysical observations, which include AOD and AE, designated Level 2 (L2). It is followed in the calculus chain by the Level 3 (L3), consisting of daily and monthly statistics of the geophysical products, in 1º x 1º latitude\longitude grid boxes. L2 aerosol products are stored in the files MOD04 (Terra) and MYD04 (Aqua).

We selected AOD at 550 nm from MODIS (both on Terra and Aqua satellites) Collection 6, L2 data level derived using the two algorithms; DB for land with highest data quality (Quality flag = 2, 3) and DT for land, corrected (Quality flag = 3). In addition, we selected the AE retrieved over land from the DB algorithm, because the DT algorithm only retrieves the AE over the ocean (Table B1 in Levy et al., 2013). We only selected the AE for the cases of high quality AOD at 550nm from DB (Quality flag = 2, 3). Table 1 lists the aerosol products used in the present study. The purpose of using the combination both satellites and DB and DT was to evaluate the reliability of the satellite AOD and AE retrievals for selecting the most appropriate data set to derive the climatology of both aerosol parameters in Cuba.

It has been established the fact that, at global scale, MODIS-retrieved aerosol size parameters using DT algorithm over land show little quantitative skill, in particular the AE (e.g., Levy et al., 2010; Mielonen et al., 2011). However, for the DB algorithm AE skill increases for moderate or high AOD (Sayer et al., 2013). Then we decided to conduct the comparison between the AE from MODIS (from DB) and the AE from the Camagüey's Sun photometer for estimating its uncertainty. It should be noted that in Collection 6 the enhanced Deep Blue algorithm has three options to calculate the AE: the traditional Deep Blue algorithm (412 nm), if the surface is vegetated uses the 470/650 nm pair; if the surface is a mixture of vegetated and non-vegetated areas, it uses all 3 wavelengths together.

2.2 *Camagüey AERONET Sun-photometer:*

Atmos. Meas. Tech. Discuss., https://doi.org/10.5194/amt-2017-318
Manuscript under review for journal Atmos. Meas. Tech.
Discussion started: 3 November 2017

Atmospheric Measurement Techniques Open Access Discussions EGU

In 2007, the University of Valladolid (UVA), Spain, and the Meteorological Institute of Cuba (INSMET) signed an agreement for conducting joint long-term aerosol research. Under this agreement, the Grupo de Óptica Atmosférica from UVA (GOA-UVA) provided a Cimel CE318 sun photometer to the Grupo de Óptica Atmosférica de Camagüey (GOAC-INSMET). The Camagüey sun photometer contributes to the Aerosol Robotic Network (AERONET) of NASA (Antuña et al., 2012). Although the annual replacement of the instrument confronted multiple delays in transportation and customs, the collected series of measurements represents a valuable dataset of the aerosol columnar optical properties in the Caribbean, allowing GOAC-INSMET and GOA-UVA to conduct preliminary aerosol research (Antuña et al, 2016).

The AERONET Cimel Sun photometers have been conducting aerosol measurements at 9 spectral narrow bands during more than two decades, producing spectral AOD and column effective particle properties (Holben et al., 1998). Its processing algorithm, based on the Beer-Lambert-Bouguer law, allows the determination of spectral AOD values at a level of uncertainty approximately of 0.01 to 0.02 (Holben et al., 1998; Eck et al., 1999). Because of this low level of uncertainty, AERONET AOD measurements commonly serve as reference values ("ground truth") for the validation of AOD measured by other remote sensing sensors (Zhao et al., 2002). AERONET AE are derived for five wavelength intervals; 340-440 nm, 380-500 nm, 440-675 nm, 440-870 nm and 500-870 nm. In the present study the AE selected is the one in the range 440-675 nm (AE_{SP}).

We used Camagüey's sun photometer Level 2.0 data as processed by AERONET, i.e. cloud screened and quality-assured (Smirnov et al., 2000), covering the period from October 7th, 2008 to August 1st, 2014. It consisted of 29,940 observations of AOD (340 to 1640nm) and AE_{SP}. We converted the individual sun photometer AOD measurements at 500 nm wavelength to AOD at 550nm, (AOD_{SP}) using the AE_{SP} from the same measurement:

$$AOD_{SP} = AOD_{500}\left(\frac{\lambda_{550}}{\lambda_{500}}\right)^{-\alpha} \tag{1}$$

where α is the AE_{SP}.

2.3 Broadband aerosol optical depth (BAOD):

Four actinometrical stations belonging to the "Diagnostic Service of the Solar Radiation in Cuba", provided the DNI measurements used to derive the BAOD (Antuña et al., 2008; 2011; GOAC, 2016). The method for determining the BAOD relays on a set of parameterizations of the most relevant extinction processes modulating the transfer of shortwave radiation in the absence of clouds (Gueymard, 1998; Garcia et al., 2015). We combined the cloud-free conditions, selecting DNI measurements under cloudiness equal or less than 1 with the cloud-free condition in the line of sight to the sun. That-free condition is satisfied selecting DNI measurements with a clear line of sight between the pyrheliometer and a region of 5° around the sun (GOAC, 2010). Table 2 lists the WMO code of the four stations, its geographical location and the available number of measurements for the periods available at each station. Figure 1 shows the geographical location of the four stations.

The main errors of the method to determine the BAOD are associated to the instrumental error and the error in the estimation of the precipitable water (PW) (Gueymard, 2013). In the first case, to guarantee the quality of the solar radiation dataset from the four actinometrical stations used in this study, including DNI, they are regularly subject of a two-step quality control (Estevan et al., 2012). The first step applies the standard procedures designed for the actinometrical instruments type Yanishevski by the former Soviet Hydro-Meteorological Service (Kirilov et al., 1957). The data passing this quality procedure are then the subject of the second step, which evaluation follows the strictest standards set by the Baseline Solar Radiation Network - BSRN (Ohmura 1998, Long and Shi, 2006; 2008; Estevan et al., 2012). Monthly mean water vapor AOD calculations, necessary for the BAOD retrieval, used monthly mean PW values at the four actinometrical stations. For Camagüey we calculated the monthly mean PW values from the sun photometer PW measurements from 2008 to 2014 (Garcia et al., 2015). For each one of the other three stations, we calculated the monthly mean PW values using the vertical integrated water vapor (kg m^{-2}) from spatially coincident ERA-Interim reanalysis from 1979 to 2013 (Barja et al., 2015). The uncertainty of the method used for the BAOD determination is in the order of 10^{-2} (Gueymard, 1998).

2.4 *Coincidence criteria for MODIS and Sun photometer measurements:*

Obtaining enough amount of satellite measurements for climatological studies at insular states represent a challenge with respect to the typical amount of data available over continental regions, like US, Europe and China for example. In response to it, we used the MODIS L2 product instead of L3 used commonly for this type of studies. We designed and applied a methodology for maximizing the available MODIS L2 measurements coincident in space and time with the sun photometer measurements. Additionally, to try to increase the amount of data, we tested the differences between Terra and Aqua L2 MODIS AOD and AE measurements to determine the possible combination of both Terra and Aqua AOD and AE measurements in a unique dataset.

Hereinafter, AODt, AODa, AODta and AOD_{SP} will denote spatio-temporally AOD from collocated MODIS (Terra, Aqua and Terra + Aqua) and AERONET sun photometer data respectively. All the “AOD” references will be

Atmos. Meas. Tech. Discuss., https://doi.org/10.5194/amt-2017-318
Manuscript under review for journal Atmos. Meas. Tech.
Discussion started: 3 November 2017

to the AOD at 550 nm wavelength, unless otherwise indicated. Similarly, AE from Terra, Aqua and Terra + Aqua derived using DB algorithm, will be denoted as AE_t, AE_a and AE_{ta}.

Because of the challenges of the low amount of potential coincident spatial and temporal AOD_t (AOD_a) with AOD_{SP} and BAOD, and of AE_t (AE_a) with AE_{SP}, explained above, we used MODIS L2 data to maximize the amount of available MODIS measurements for the comparison. Hereinafter we named those measurements "single observation values"; using the same denomination for the instantaneous sun photometer measurements on each day and for the hourly pyrheliometer measurements. Another way to increase the amount of data was to combine AOD_t and AOD_a (AOD_{ta}) for the comparison with AOD_{SP} and BAOD; and the combined AE_t and AE_a (AE_{ta}) for the comparison with AE_{SP}. In these cases, different measurements of AOD_{SP} and BAOD match AOD_t and AOD_a because the time difference established for coincidence (± 30 min) is lower than the difference between the Terra and Aqua daily overpass times.

The spatial coincidence criteria was granted by selecting all AOD_t and AOD_a measured inside the 25 km radius around the sun photometer site for the entire period of data from each satellite sensor. Table 3 shows the amount of spatial coincident information for non-negative AOD_t and AOD_a. It shows the amount of data available or the entire period 2011 to 2015 and for 2008 to 2014, the period of the available sun photometer measurements. The available measurements from Terra are at least twice the number of measurements from Aqua for both periods, causing the same balance of measurements with the sun photometer as it will be shown below. The higher amount of available data from Terra with respect to Aqua is associated to the different overpass times of both satellites over Cuba. Figure 2 shows that Terra overpasses occur in the middle to late morning before convective activity begins, while Aqua overpasses take place in the early afternoon when convection already began causing a higher amount of observations to be discarded in AOD retrievals due to the presence of clouds.

2.4.1 *Single observation values:*

All Aqua and Terra overpass times in a radius of 25 km around Camagüey for the periods 2001 to 2015 (Terra) and 2002 to 2015 (Aqua) are shown on figure 2. Overpass times, defined by the maximum and minimum values of all the 25 km spatially coincident MODIS measurements, are 10:12 -11:49 (LT) for Terra and 12:47 – 14:20 (LT) for Aqua. In addition, figure 2 shows the diurnal frequency of sun photometer measurements from 2008 to 2014. Also the diurnal frequency of the BAOD measurements for Camagüey for the period 1981 to 2015. Note that the

BAOD histogram shows only hourly frequency values, because that is the time interval between the manual pyrheliometric measurements.

For each day, we compared the corresponding time of each individual sun photometer measurement with the time of each individual AOD_t and AOD_a measurements the same day located in a radius of 25 km around the sun photometer site and in the time window of ± 30 minutes between both measurements. The former process of selection includes, for each satellite, the values of AOD_t and AOD_a derived both with the DB and DT processing algorithms separately, producing four independent bulk datasets, two for Aqua and two for Terra, coincident spatially inside 25 km radius around the sun photometer location, an area of almost 2,000 km^2. Then we identified four different cases of daily coincident data in the bulk coincident datasets. The first consisted of days with only one AOD_{SP} value and one AOD_t (AOD_a) coincident value. The second, only one AOD_{SP} value coincident with multiple AOD_t (AOD_a) values each day. In the third case only one AOD_t (AOD_a) value, coincide with multiple AOD_{SP} values. Finally, the fourth case consisted of multiple AOD_{SP} values coincident with multiple AOD_t (AOD_a) values.

The selection of the coincident cases for the comparison was then conducted, case by case. In the first case we selected all the cases. In the second case, because of the MODIS instruments spatiotemporal sampling geometry, the differences in time between the MODIS and sun photometer measurements are in the order of one minute. Then only the criteria of the minimum distance between the positions of the AOD_t (AOD_a) and the sun photometer was applied to determine the pair of coincident values, thus granting no repeated AOD_{SP} and AOD_t (AOD_a) values being selected. In the third case because it consists of only one AOD_t (AOD_a) measurement and multiple AOD_{SP} measurements, the distance is the same, hence the criteria of selection was the minimum of the time differences between AOD_{SP} and AOD_t (AOD_a) measurements. The fourth case, the most complicated one, allowed the application of both criteria; the minimum in distance and time. We tested the influence of the order of application of both criteria and it produced no differences in the amount coincident data.

2.4.2 *Daily mean values in the ± 30 minute interval around MODIS overpass time:*

Another approach for the comparison of AOD_{SP} and AOD_t (AOD_a) measurements consists of time averages of the AOD_{SP} values in the interval of ± 30 minutes with respect to MODIS instruments overpass time. We averaged the AOD_t and AOD_a measurements located in a radius of 25 km around the sun photometer site for the time interval of ± 30 minutes around the Terra (Aqua) overpass time respectively for the same day (Sayer et al., 2014). We applied a similar approach to calculate daily means AE_A, AE_t and AE_a. Then for each one of those days we calculated the daily mean AOD_{SP} for the time interval of ± 30 minutes around the Terra (Aqua) overpass time respectively. The procedures described above generated a series of daily means AOD_{SP} vs. AOD_t (AOD_a) and AE_{SP} vs AE_t (AE_a). Combining the former generated series of AOD for Terra and Aqua we produced the coincident Terra + Aqua daily means dataset. We followed a similar procedure for the AE coincident Terra + Aqua dataset. The term *daily mean AOD* will be used hereinafter although it does not represent exactly a daily average. It refers only to an hourly average centered on the MODIS overpass time.

2.5 *Statistics*

The statistics used in the present study are the ones commonly used (e.g., Sayer et al., 2014). They are the root mean squared error (RMSE), mean absolute error (MAE), median bias (BIAS), the linear correlation coefficient (R), the number of coincident MODIS and sun photometer cases (Cases) and the fraction (f) of the MODIS/AERONET AOD retrievals in agreement within the expected uncertainty. The expected uncertainty, defined as a one standard deviation confidence interval, appears in the equation 2 (Sayer et al., 2014):

$$EE_{DT} = \pm(0.05 + 0.15\,AOD) \qquad (2)$$

We used AOD_t (AOD_a) expected uncertainty defined in equation 2, determined for the DT algorithm, also for estimating the uncertainty of AOD_t (AOD_a) when the DT algorithm is applied, to allow the performance of DB and DT to be compared more directly (Sayer et al., 2014).

The RMSE, MAE, BIAS, R and f were evaluated for the complete set of coincident AOD_t, AOD_a, AOD_{ta} with AOD_{SP} ; AOD_t, AOD_a, AOD_{ta} with BAOD and BAOD with AOD_{SP}; AE_t, AE_a, AE_{ta} with AE_{SP}. In addition, we evaluated those statistics at monthly scales for the comparison of AOD_{SP} with AOD_t, AOD_a, AOD_{ta}, and BAOD. In addition, we calculated the time frequencies and histograms of the magnitudes of AOD_t, AOD_a, $AOD_{ta,}$ AOD_{SP}, BAOD, AE_t AE_a, AE_{ta} and AE_{SP} measurements.

3. Results and Discussion:

3.1 *Comparison of AOD retrievals from sun photometer and MODIS satellite instruments*

3.1.1 *Daily means*

Figure 3 shows the scatter plot of the daily means AOD values from the sun photometer and Terra (Aqua) MODIS instruments for DB and DT algorithms. Table 4 shows the statistics of the comparison of daily mean AOD_t (AOD_a) with AOD_{SP}. For AOD_t RMSE and MAE are lower for the DT than for DB algorithm. In addition, the magnitude of the BIAS is lower for DT than for DB and its sign is the same for both DT and DB. The sign and magnitude of the BIAS for DB demonstrate that the daily mean AOD_t from DB algorithm are larger than the daily mean AOD_{SP}. However, in the case of DT the low BIAS shows that there are not predominant higher values between the daily mean AOD_t from DT algorithm and AOD_{SP}. Up to 80% of AOD_t values derived with DT are inside the expected error margins, while this statistic decreased to 66% for DB. The correlation coefficient R shows no differences between DT and DB and f shows a value of 80% for DT, decreasing to 76 % for DB. In the case of AOD_a, RMSE and MAE show almost no difference for DB and DT while the BIAS is negative for DB and positive for DT, with lower absolute value for DT as in the case of AOD_t.

From the results described above it is evident that the monthly means AOD_t and AOD_a derived using the DT algorithm agree better with the AOD_{SP} than the ones derived using the DB algorithm. In addition, the similar values of the statistics for both AOD_t and AOD_a derived with DT support the combination of the monthly mean AOD_{ta} in a unique dataset for studies ranging from daily to climatological temporal scales. The last two columns in table 4 report the statistics for such combined AOD_{ta} dataset. As expected, the DT algorithm shows better agreement between combined AOD_{ta} dataset with AOD_{SP} than DB.

3.1.2 *Single observation values*

The results of the comparison of the single observations measurements of AOD_t (AOD_a) with AOD_{SP} are in table 5. The magnitudes of the statistics on table 5 are, in general, similar to the results shown in table 4 for the comparison of the daily means. The single observations AOD_t derived with DT also shows better results than the ones derived with DB but that is not the case for AOD_a. The BIAS shows that DB algorithm also produces higher values of the single observations mean AOD_t (AOD_a) than the single observations AOD_{SP} values. On the other side DT produces lower values of the single observations mean AOD_t (AOD_a) than the individual AOD_{SP} values. The absolute magnitude of the overestimation produced by DB is higher than the underestimation produced by DT. The AOD_t and AOD_a derived with DT show higher percent values inside the expected error margins than the same variables derived using DB.

The similitude of the statistics for DT both for AOD_t and for AOD_a, also adds the intra-daily temporal scale to the already determined range of temporal scales from the comparison of daily means AOD_t and AOD_a with AOD_{SP}. The last two columns on table 5 report the statistics for the comparison of the single observations values of the combined AOD_{ta} dataset with the single observations values of AOD_{SP}. Its values are quite similar to the ones on table 4 for the daily mean AOD_t (AOD_a) comparison with AOD_{SP}.

Atmos. Meas. Tech. Discuss., https://doi.org/10.5194/amt-2017-318
Manuscript under review for journal Atmos. Meas. Tech.
Discussion started: 3 November 2017

Atmospheric Measurement Techniques Discussions

3.1.3 *Monthly single observations.*

Figure 4 shows the monthly means and statistics resulting from the comparison between AOD_{SP} and AOD_{ta} for both DB and DT algorithms. Figure 4a shows the multiannual monthly means from the combined AOD_{ta} with AOD_{SP} when the MODIS DB and DT algorithm are used. We combined the two coincident sets of measurements of AOD_{t} coincident with AOD_{SP} and from AOD_{a} coincident with AOD_{SP} to produce the combined AOD_{ta} with AOD_{SP} dataset. Similarly, the coincident Camagüey's sun photometer dataset AOD_{SP} was generated from the union of both individually coincident AOD_{SP} datasets with AOD_{a} and AOD_{t}, which were independent as it was explained above, because the differences in overpass time between Terra and Aqua is higher than the time difference established for coincidence (± 30 min). Monthly mean AOD_{ta} derived with DT algorithm shows the best match with monthly mean AOD_{SP}.

The monthly RMSE and MAE plots, on figures 3b and 3c, show increases in general, with the increase of the AOD_{ta} for the DB algorithm. These results are consistent with the fact that the AOD uncertainty depends on the AOD itself (see eq. 2). The peaks in March in both RMSE and MAE are present also in the RMSE and MAE results for AOD_{t} and AOD_{a} separately and the amount of cases available for the statistics is among the highest of all the months seen on tables S1 and S2 (see supplement 01). We have no explanation for it.

Tabulated results of the comparison between AOD_{t}, AOD_{a} and AOD_{ta} with AOD_{SP} at monthly scale, showing also better results for DT, table S1, than for DB, table S2, both on supplement tables. Here we will discuss only the results of the joint AOD_{ta} dataset using both the DT and DB algorithms for the retrievals.

In figures 3d, the BIAS for the DT algorithm is positive from December to May, a period of the year with predominant lower values of AOD_{ta} and AOD_{SP}. During this period, AOD_{ta} underestimates the AOD_{SP}. Then the BIAS becomes negative from June to November, which is the period of the year when the arrival of Saharan dust to the Caribbean basin occur. At the same time the BIAS of the AOD_{ta} derived with the DB algorithm is negative the whole year, with higher absolute values magnitudes than the ones from DT algorithm.

The correlation coefficient, R, on figure 4e is the statistics showing almost the same agreement for the DB and DT algorithm. However, DT shows a higher number of R-values bearing higher magnitudes. R magnitudes remain over 0.5 almost the year around except in December and January when lower AOD values occur.

The fraction of the AOD_{ta} (f) shown on figure 4f, in agreement with AOD_{SP} within the expected uncertainty, shows its higher values over 80 % from November to January, in general for both algorithms. This is the period of the year with the lower monthly mean values of both AOD_{ta} and AOD_{SP}. During the rest of the year, including the period of the Saharan dust arrivals, it shows its lower values between 60 % and 75 % for the DT algorithm while for DB values below 50 % occur in four of the month between June and October. The blue discontinuous line at f = 68 % denotes one standard deviation confidence interval, selected for the definition of EE. The values of f above that value mean the algorithm works well than expected. All the statistics demonstrate that the DT algorithm performs better than DB for the region of study.

3.2 *Comparison of Ångström Exponent by sun photometer and MODIS satellite instruments:*

Figure 5 shows the frequency distribution of the AE_{SP} as well as AE_t and AE_a. We used the AE_a and AE_t derived using the DB algorithm measured in a radius of 25 km around the sun photometer for the whole 2001 – 2015 period (2002 - 2015 in the case of Aqua). A maximum frequency for both AE_t and AE_a appears for the values of AE = 1.5 followed by a secondary maximum at AE = 1.8. The first of them, 1.5, is a regional default value for AE_t and AE_a (Hsu et al., 2013; Sayer et al., 2013) assumed by DB in case of low AOD values (AOD_t or AOD_a < 0.2) because of the lack of information on this parameter. The second one is associated with the fact that the AE_t and AE_a values allowed by the aerosol optical models in Collection 6 are constrained between 0 and 1.8 to avoid unrealistic values (Sayer et al., 2013).

Table 6 shows the results of the comparison of coincident AE_t and AE_a measurements in radius of 25 km around the Camagüey's sun photometer and ± 30 minutes with AE_{SP} measurements. We classified the AE from the two MODIS instruments and the sun photometer coincident values in three groups. The first one considers the daily individual coincident AE_t, AE_a with AE_{SP}. The second one excludes from the daily individual coincident AE_t and AE_a with AE_{SP} the cases of AE_t and AE_a equal to 1.5 or 1.8 value. The third one compares the daily mean values of daily individual coincident AE_t and AE_a with AE_{SP}, including the cases of AE_t and AE_a equal to 1.5 or 1.8 values. We took into account also the combined coincident AE_{ta} with AE_{SP} for the three cases.

Scatter plots are in figure 1S in the supplements. Statistics on table 6 for the three cases the RMSE, MAE and BIAS statistics are in the same order of magnitudes. In addition, the magnitude of R is below 0.5 and negative for the three cases. The comparison showed the low quantitative skill of the AE_t and AE_a for this site providing numeric magnitudes of it. One factor contributing to this result is that the AE from AERONET has large uncertainty in low-AOD conditions, because the AE is a gradient between two small numbers (Wagner and Silva, 2008). Another factor could be the poor performance that the DB algorithm showed in the comparison with AOD_{SP}.

Atmos. Meas. Tech. Discuss., https://doi.org/10.5194/amt-2017-318
Manuscript under review for journal Atmos. Meas. Tech.
Discussion started: 3 November 2017

3.3 Comparison of AOD between MODIS products and BAOD for the four Cuban actinometrical stations.

Two main facts limit the number of available BAOD values coincident in time with AOD_t and AOD_a. The manual DNI measurements conducted hourly used to derive BAOD; and the required condition for these measurements to take place under a clear line of sight between the pyrheliometer and a region of 5° around the Sun. Consequently, only one BAOD could coincide each day with AOD_t, and another one with AOD_a because of the time coincidence criteria. Table 7 list the number of coincident AOD_t, $AOD_{a,}$ AOD_{ta} measurements in space and time with BAOD both for DB and for DT algorithms for each one of the actinometrical stations. Because the amount of coincident measurements at each station is low, we decided to combine all the pairs of AOD_{TE}, AOD_a and AOD_{ta} coincident with BAOD in the four sites together to conduct the comparison. In addition, we did not considered the very few cases with values of BAOD > 0.5, around 1 %, of all the cases.

Table 8 contains almost the same statistics used in previous comparison satellite-sun photometer data (see Table 4), both for DB and for DT algorithms for the four actinometrical stations together. The scatter plot of the BAOD vs. AOD_t, AOD_a, and AOD_{ta} appears in figure 6, The only statistic not included in table 8 is f, the fraction of the MODIS/AERONET AOD retrievals in agreement within the expected uncertainty, because such uncertainty has still to be established for BAOD. We highlighted the best performing algorithm in bold for each one of the statistics. The AOD_a derived with the DB algorithm performs better than the other three combinations of AOD_t, AOD_a, for DT and DB according all the four statistics, except for the BIAS, where the best performing is still the DB algorithm but for AOD_t. However, in general the RMSE, MAE and for AOD_t, AOD_a, AOD_{ta} derived with both DB and DT algorithms remain in the same order of magnitude. The BIAS shows an almost similar behavior except for its best performing value.

3.4 Comparing BAOD from actinometrical data and sun photometer:

Theoretical studies have shown that the best agreement between BAOD and AOD_{SP} occurs at the wavelengths about 700 nm (Blanchet, 1982; Molineaux et al., 1998). In addition, the Molineaux et al., (1998) study reports an empirical validation finding that measured BAOD and AOD at 700 nm had similar values. We found no literature reports about BAOD validations with AOD_{SP} at each one of the AERONET sun photometer wavelengths.

At Camagüey, using the 715 coincident measurements (± 30 minutes) of BAOD and AOD_{SP} in the period from 2008 to 2013, we calculated the coefficients of determination (R^2) between BAOD and AOD_{SP} at each sun photometer wavelength. Results showed the higher values of R^2 (about 0.45) at 675 and 500 nm (Garcia et al., 2015).

Atmos. Meas. Tech. Discuss., https://doi.org/10.5194/amt-2017-318
Manuscript under review for journal Atmos. Meas. Tech.
Discussion started: 3 November 2017

The comparison we report here includes those same BAOD and AOD_{SP} at each sun photometer wavelengths plus 162 pairs of coincident measurements from 2014.

Table 9 shows the statistics of the comparison between BAOD with AOD_{SP} at the eight wavelengths measured in Camagüey. Corresponding scatter plots are in figure 2S in the supplements. The amount of cases is the same at all wavelengths with the exception of 1640 nm. Two out of six CIMEL sun photometers employed at Camagüey site between 2008 and 2014 had a 1240 nm channel instead of the most common 1640 nm. At 500 nm R^2 is 0.48 (R = 0.69) while at 675 nm and 400 nm wavelengths the R^2 has the same value of 0.46 (R = 0.68), very similar among the three wavelengths and with the results reported by Garcia et al., (2015) with a slightly less data. However, the other three statistics show notorious differences. The best performing value for each statistic is in bold, belonging to the 500 nm wavelength follow by the 675 nm and 440 nm in that order. After this comparison, we can estimate the uncertainty of the BAOD to be about 0.04 larger than the sun photometer uncertainty, i.e. 0.06 in total and the best correspondence takes place at the 500nm wavelength.

4. Summary and conclusions

The study address the comparisons of different sources of AOD and AE from ground-based sun photometer (AERONET level 2.0 data), MODIS instruments (Terra, Aqua, and Terra + Aqua) and retrievals from direct normal irradiance observations in Cuba for a long period. Results of comparison between spatial and temporal coincident daily mean values in the ± 30 minutes interval around MODIS overpass time AOD_{SP} vs. AOD_t and AOD_a show better performance for the Dark Target (DT) algorithm. We found little differences between AOD_t and AOD_a justifying the combination of AOD_t and AOD_a measurements in one dataset. When we conducted the comparison between daily individual spatial and temporal coincident AOD_{SP} vs. AOD_t and AOD_a we found similar results. For both spatial and temporal coincident daily means and daily individual observations of AOD_{SP} vs. AOD_t and AOD_a, the correlation coefficient R is equal or higher than 0.70 for Deep Blue (DB) and DT algorithms. However, the most notorious result is the fact that the portion of AOD_t and AOD_a values within the expected error margins ($0.05±0.15·AOD$) is higher for DT than for DB both when we used single observations and daily means values. That is an important criterion to take into account for the selection of the AOD_t and AOD_a data to calculate the aerosol climatology over Cuba.

The statistical evaluation of multiannual monthly means of the daily individual coincident AOD_{ta} and AOD_{SP} reveals a direct relation between the RMSE and MAE values and the monthly mean values of AOD_{ta}. The BIAS and fraction of data within the uncertainty margins (f) show an inverse relation with the monthly mean values of AOD_{ta}.

Daily mean Ångström exponents AE_t, AE_a and AE_{ta} do not show a good agreement with daily mean and daily individual spatial and temporal coincident AE_{SP} values. This result corroborates the limitation of the MODIS derived AE in general.

In the comparison of BAOD vs. AOD_t, AOD_a, AOD_{ta} the AOD_a the errors are of the same order of magnitude than the average values, in general. It is noteworthy that for the AOD satellite products the statistics are similar for the sun photometer AOD and the BAOD. This result points out the potential of BAOD to be a reliable source of aerosol information in the places lacking sun photometer or any other surface measurement. This conclusion is reinforced by the results of the comparison of BAOD with AOD_{SP} at all the eight individual sun photometer wavelengths, showing better agreement in the spectral bands between 400 and 675 nm with the better result at 500 nm and typical uncertainty about 0.04-0.06 in this spectral range.

5. Acknowledgements:

This work has been supported by the Cuban National Program "Meteorology and sustainable development for Cuba" research grant P211LH007-20 and by the Joint Agreement between the University of Valladolid, Spain, and the Cuban Meteorological Institute for aerosol research. JCAM wants to thank Dr. Loraine Remer and Dr. Andrew Sayer for their contributions to the understanding of MODIS algorithms. This research has received funding from the European Union's Horizon 2020 Research and Innovation Program under grant agreement No 654109 (ACTRIS-2). We acknowledge the funding by MINECO (CTM2015-66742-R) and Junta de Castilla y León (VA100U14).

6. References:

Antuña, J. C., Fonte, A., Estevan, R., Barja, B., Acea, R., Antuña Jr.: J.C., Solar radiation data rescue at Camagüey, Cuba, *Bull. Am. Meteorol. Soc*, **89**, 1507–1511. http://dx.doi.org/10.1175/2008BAMS2368.1, 2008.

Antuña J. C., Hernández, C., Estevan, R., Barja, B., Fonte, A., Hernández, T., Antuña Jr, J. C.: Camagüey's solar radiation rescued dataset: preliminary applications, *Óptica Pura y Aplicada*, **44** (1), 43-48, 2011

Antuña, J. C., Estevan, R., Barja, B.: Demonstrating the Potential for First-Class Research in Underdeveloped Countries: Research on Stratospheric Aerosols and Cirrus Clouds Optical Properties, and Radiative Effects in Cuba (1988–2010), *Bull. Amer. Meteor. Soc.*, **93**, 1017–1027. http://dx.doi.org/10.1175/BAMS-D-11-00149.1, 2012.

Antuña-Marrero, J. C., De Frutos Baraja, A., Estevan Arredondo, R.: Joint aerosol research between Cuba and Spain proves fruitful, *EOS*, **97**, doi:10.1029/2016EO060125, 2016.

Atmos. Meas. Tech. Discuss., https://doi.org/10.5194/amt-2017-318
Manuscript under review for journal Atmos. Meas. Tech.
Discussion started: 3 November 2017

Atmospheric Measurement Techniques
Open Access
Discussions

Barja, B., Rosas, J., Estevan, R.: Caracterización del contenido integral del vapor de agua atmosférico sobre Cuba obtenido mediante mediciones y modelación, *Scientific Report*, Grant 200.04070, 77 pp. (*In Spanish, unpublished*), 2015.

Blanchet, J. P.: Application of the Chandrasekhar mean to aerosol optical parameters, *Atmos. Ocean*, **20**, 189–206, 1982.

Eck, T., Holben, B., Reid, J. Dubovik, O.: Wavelength dependence of the optical depth of biomass burning, urban, and desert dust aerosols. *J. Geophys. Res.*, **104**, 31333_31349, 1999.

Estevan R., Antuña, J.C., Barja, B., Hernández, C.E., Hernández, T., García, F., Rosas, J., Platero, I. Y.: Climatología de la Radiación solar en Camagüey 1981 – 2010, *Scientific Report*, Grant 01301216, 41 pp. (*In Spanish, unpublished*), 2016.

Fonte, A., Antuña, J.C.: Caracterización del espesor óptico de banda ancha de los aerosoles troposféricos en Camagüey, Cuba, *Revista Cubana de Meteorología*, **17**, No. 1, pp. 15-26, 2011.

García, F., Estevan, R., Antuña-Marrero, J. C., Rosas, J., Platero, I. Y., Antuña-Sánchez, J., C. Díaz, N.: Determinación de la Línea Base del Espesor Óptico de Aerosoles de Banda Ancha y comparación con datos de fotómetro solar. *Óptica Pura y Aplicada*, **48**(4), 249-258.DOI: 10.7149/OPA.48.4.249, 2015.

GOAC: Manual de Observaciones Actinométricas, 37 pp. (*In Spanish, unpublished*), 2010.

GOAC: Servicio de Diagnóstico de la Radiación Solar para Cuba. http://www.goac.cu/actino/, 2016.

Gueymard, C.A.: Turbidity determination from broadband irradiance measurements: A detailed multicoefficient approach. *J. Appl. Meteorol*. **37**: 414-435, 1998.

Gueymard, C. A. Aerosol turbidity derivation from broadband irradiance measurements: Methodological advances and uncertainty analysis. *Solar 2013 Conf.*, Baltimore, MD, American Solar Energy Soc., 8 pp., 2013.

Holben, B. N., Tanre, D., Smirnov, A., Eck, T. F., Slutsker, I., Abuhassan, N., Newcomb, W. W., Schafer, J., Chatenet, B., Lavenue, F., Kaufman, Y. J., Castle, J. V., Setzer, A., Markham, B., Clark, D., Frouin, R., Halthore, R., Karnieli, A., O'Neill, N. T., Pietras, C., Pinker, R. T., Voss, K., Zibordi, G.: An emerging ground-based aerosol climatology: Aerosol optical depth from AERONET, *J. Geophys. Res.*, **106**, 12,067–12,097, 2001.

Hsu, N. C., Tsay, S. C., King, M. D., Herman, J. R.: Aerosol Properties Over Bright-Reflecting Source Regions, *IEEE T. Geosci. Remote*, **42**, 557–569, doi:10.1109/TGRS.2004.824067, 2004.

Atmos. Meas. Tech. Discuss., https://doi.org/10.5194/amt-2017-318
Manuscript under review for journal Atmos. Meas. Tech.
Discussion started: 3 November 2017

Hsu, N. C., Tsay, S. C., King, M. D., Herman, J. R.: Deep blue retrievals of Asian aerosol properties during ACE-Asia, *IEEE T. Geosci. Remote*, **44**, 3180–3195, doi:10.1109/TGRS.2006.879540, 2006.

Hsu, N. C., Jeong, M.-J., Bettenhausen, C., Sayer, A. M., Hansell, R., Seftor, C. S., Huang, J., Tsay, S.-C.: Enhanced Deep Blue aerosol retrieval algorithm: the second generation, *J. Geophys. Res.*, **118**, 9296–9315, doi:10.1002/jgrd.50712, 2013.

IPCC: Climate Change 2013. The Physical Science Basis –Contribution of Working Group I to the Fifth Assessment Report of the Intergovernmental Panel on Climate Change, Stocker TF, Qin D, Plattner G-K, Tignor M, Allen SK, Boschung J, Nauels A, Xia Y, Bex V, Midgley PM. (eds). Cambridge University Press: Cambridge, UK and New York, NY, 2013.

Kaufman, Y. J., Tanre, D., Remer, L. A., Vermote, E. F., Chu, A., Holben, B. N.: Operational remote sensing of tropospheric aerosol over land from EOS moderate resolution imaging spectroradiometer, *J. Geophys. Res.*, **102**, 17051–17068, doi:10.1029/96JD03988, 1997.

Kirilov, T. B., Vlasov, Yu. B., Flaum, M. Ya.: Manual para la operación e instalación de instrumentos de radiación solar, Ed.Guidrometeoizdat, Leningrad, 124 pp. (In Russsian), 1957.

Knippertz, P., Stuut, J.-B.W., 2014. Chapter 1 Introduction. In: Knippertz, P., Stuut, J.-B.W. (Eds.), Mineral Dust: A Key Player in the Earth System. Springer, New York, pp. 1–14, http://dx.doi.org/10.1007/978-94-017-8978-3, 2014

Levy, R. C., Remer, L. A., Kleidman, R. G., Mattoo, S., Ichoku, C., Kahn, R., Eck, T. F.: Global evaluation of the Collection 5 MODIS dark-target aerosol products over land, *Atmos. Chem. Phys.*, **10**, 10399-10420, doi:10.5194/acp-10-10399-2010, 2010.

Levy, R. C., Mattoo, S., Munchak, L. A., Remer, L. A., Sayer, A. M., Patadia, F., Hsu, N. C.: The Collection 6 MODIS aerosol products over land and ocean, *Atmos. Meas. Tech.*, **6**, 2989-3034, doi:10.5194/amt-6-2989-2013, 2013.

Long, C.N., Shi, Y.: The QCRad Value Added Product: Surface Radiation Measurement Quality Control Testing, Including Climatology Configurable Limits, Office of Biological and Environmental Research, U.S. Department of Energy, pp. 69, 2006.

Long, C.N., Shi, Y.: An Automated Quality Assessment and Control Algorithm for Surface Radiation Measurements. *The Open Atmospheric Science Journal*, **2**, 23-37,2008.

Atmos. Meas. Tech. Discuss., https://doi.org/10.5194/amt-2017-318
Manuscript under review for journal Atmos. Meas. Tech.
Discussion started: 3 November 2017

Atmospheric Measurement Techniques Discussions

Martínez, E., Campos, A., Borrajero, I., Vázquez, A.: Algunos índices de turbidez del aire en la Ciudad de la Habana, *Revista Cubana de Meteorología*, **1** (1), pp. 57-60, 1988.

Mielonen, T., Levy, R. C., Aaltonen, V., Komppula, M., de Leeuw, G., Huttunen, J., Lihavainen, H., Kolmonen, P., Lehtinen, K. E. J., Arola, A.: Evaluating the assumptions of surface reflectance and aerosol type selection within the MODIS aerosol retrieval over land: the problem of dust type selection, *Atmos. Meas. Tech.*, **4**, 201–214, doi:10.5194/amt-4-201-2011, 2011.

Molineaux, B., Ineichen, P., O'Neill, N.: Equivalence of pyrheliometric and monochromatic aerosol optical depths at a single key wavelength, *App. Opt.* **37**, 30, 7008-7018. http://dx.doi.org/10.1029/1999JD901105, 1998.

Ohmura, A., Dutton, E., Forgan, B., Froehlich, C., Gilgen, H., Hegner, H., Heimo, A., Koenig-Langlo, G., McArthur, B., Mueller, G., Philipona, R., Pinker, R., Whitlock, C., Wild, M.: Baseline Surface Radiation Network (BSRN/WCRP), a new precision radiometry for climate research. *Bull. Am. Meteorol. Soc*., **79**, 2115-2136, 1998.

Prospero, J. M., Lamb, P. J.: African droughts and dust transport to the Caribbean: Climate change implications. *Science*, **302**, 1024–1027, 2003.

Prospero, J. M., Mayol-Bracero, O. L.: Understanding the transport and impact of African dust on the Caribbean Basin, *Bull. Am. Meteorol. Soc.*, **94**(9), 1329–1335, 2013.

Prospero, J. M., Collard, F.-X., Molinié, J., Jeannot, A.: Characterizing the annual cycle of African dust transport to the Caribbean Basin and South America and its impact on the environment and air quality, *Global Biogeochem. Cycles*, **29**, 757–773, doi:10.1002/2013GB004802, 2014.

Sayer, A. M., Hsu, N. C., Bettenhausen, C., Jeong, M.-J.: Validation and uncertainty estimates for MODIS Collection 6 "Deep Blue" aerosol data, *J. Geophys. Res. Atmos.*, **118**, 7864–7872, doi:10.1002/jgrd.50600, 2013.

Sayer, A.M., Munchak, L. A., Hsu, N. C., Levy, R. C., Bettenhausen, C., Jeong, M.-J.: MODIS Collection 6 aerosol products: Comparison between Aqua's e-Deep Blue, Dark Target, and "merged" data sets, and usage recommendations, *J. Geophys. Res. Atmos.*, **119**, 13,965–13,989, doi:10.1002/2014JD022453, 2014.

Seinfeld, J. H. and S. N. Pandis.: Atmospheric chemistry and physics : from air pollution to climate change. 3rd edition. John Wiley & Sons, Inc., ISBN: 9781118947401, 1120 pp., 2016.

Smirnov, A., Holben, B. N., Eck, T. F.. Dubovik, O., Slutsker, I.: Cloud-screening and quality control algorithms for the AERONET database, *Remote Sens. Environ.*, **73**(3), 337–349, 2000.

Atmos. Meas. Tech. Discuss., https://doi.org/10.5194/amt-2017-318
Manuscript under review for journal Atmos. Meas. Tech.
Discussion started: 3 November 2017

Swap, R., Garstang, M., Greco, S., Talbot, R., Kallberg, P.: Saharan dust in the Amazon basin. *Tellus*, **44B**, 133–149, 1992.

Tanre, D., Kaufman, Y. J., Herman, M., Mattoo, S.: Remote sensing of aerosol properties over oceans using the MODIS/EOS spectral radiances, *J. Geophys. Res.*, **102**, 16971–16988, 1997.

Wagner, F., and Silva A. M.: Some considerations about Ångström exponent distributions. *Atmos. Chem. Phys.*, **8**, 481–489, 2008.

Yu, H., , M. Chin, T. Yuan, H. Bian, L. A. Remer, J. M. Prospero, A. Omar, D. Winker, Y. Yang, Y. Zhang, Z. Zhang and C. Zhao, The fertilizing role of African dust in the Amazon rainforest: A first multiyear assessment based on data from Cloud-Aerosol Lidar and Infrared Pathfinder Satellite Observations, *Geophys. Res. Lett.*, **42**, 1984–1991, doi:10.1002/2015GL063040, 2015.

Zhao, T. X.-P., Stowe, L. L., Smirnov, A., Crosby, D., Sapper, J., McClain, C. R.: Development of a global validation package for satellite oceanic aerosol optical thickness retrieval based on AERONET observations and its application to NOAA/NESDIS operational aerosol retrievals, *J. Atmos. Sci.*, **59**, 294– 312, 2002.

Atmos. Meas. Tech. Discuss., https://doi.org/10.5194/amt-2017-318
Manuscript under review for journal Atmos. Meas. Tech.
Discussion started: 3 November 2017

Atmospheric Measurement Techniques Discussions
Open Access
EGU

Tables:

Table 1: Aerosol products from MODIS Collection 6 dataset used in the present study

Product	Description
Deep_Blue_Aerosol_Optical_Depth_550_ Land_Best_Estimate	Deep Blue AOT at 0.55 micron for land with higher quality data (Quality flag=2,3)
Deep_Blue_Angstrom_Exponent_Land	Deep Blue Angstrom Exponent for land with all quality data (Quality flag=1,2,3)
Optical_Depth_Land_And_Ocean	AOT at 0.55 micron for both ocean (Average) (Quality flag=1,2,3) and land (corrected) (Quality flag=3)

Table 2: Information about the Cuban actinometrical stations operating under the Solar Radiation Diagnostic Service (SRDS). Available BAOD number of observations included in column 6 and the period they cover in the last column.

Code	Station Name	Latitude	Longitude	Height (m)	No. Obs.	Period
78355	Camagüey (CMW)	21.42	-77.85	122 m	2495	2001-2015
78330	Jovellanos (JVN)	22.80	-81.14	23 m	1182	2010-2015
78342	Topes de Collantes (TPC)	21.92	-80.02	766 m	1358	2011-2015
78321	Santa Fé (LFE)	21.73	-82.77	32 m	1756	2011-2015

Table 3: Available non-negative AOD_a, AOD_t, AE_t and AE_a spatially coincident with Camagüey sun photometer in a radius of 25 km for each retrieval algorithms, DB and DT. The entire period 2001-2015 is shown as well as the period AOD_{SP} and AE_{SP} are available, 2008-2014.

Period	**2001-2015**			**2008-2014**		
Algorithm	**DB**		**DT**	**DB**		**DT**
Parameter	**AOD**	**AE**	**AOD**	**AOD**	**AE**	**AOD**
Terra	6884	8111	6311	3418	4024	3166
Aqua	2445	3909	2869	1329	1534	2093

Atmos. Meas. Tech. Discuss., https://doi.org/10.5194/amt-2017-318
Manuscript under review for journal Atmos. Meas. Tech.
Discussion started: 3 November 2017

Atmospheric Measurement Techniques Discussions
Open Access
EGU

Table 4: Statistics of the comparison between daily means AOD_t (AOD_a) with AOD_{SP}. In addition, the statistics for the comparison between the combined AOD_{ta} with AOD_{SP} is shown in the last two columns.

	AOD_{SP} vs. AOD_t		**AOD_{SP} vs. AOD_a**		**AOD_{SP} vs. AOD_{ta}**	
	DB	**DT**	**DB**	**DT**	**DB**	**DT**
RMSE	0.084	0.060	0.065	0.062	0.078	0.061
MAE	0.062	0.045	0.046	0.047	0.056	0.046
BIAS	-0.053	-0.001	-0.033	0.006	-0.046	0.002
R	0.730	0.729	0.785	0.779	0.741	0.753
f	0.656	0.803	0.763	0.795	0.694	0.800
Cases	311	335	169	254	480	589

Table 5: Statistics of the comparison between single observation AOD_t and AOD_a with AOD_{SP}.

	AOD_{SP} vs. AOD_t		**AOD_{SP} vs. AOD_a**		**AOD_{SP} vs. AOD_{ta}**	
	DB	**DT**	**DB**	**DT**	**DB**	**DT**
RMSE	0.081	0.061	0.063	0.064	0.076	0.062
MAE	0.059	0.046	0.044	0.050	0.054	0.047
BIAS	-0.048	0.007	-0.027	0.017	-0.042	0.010
R	0.716	0.701	0.817	0.794	0.744	0.742
f	0.664	0.773	0.773	0.784	0.699	0.777
Cases	880	900	419	500	1299	1400

Table 6: Statistics of the comparison between AE_t, AE_a and AE_{ta} with AE_{SP}.

	Single observations			**Single observations (Except AE 1.5 & 1.8)**			**Daily Means**		
	AE_t	**AE_a**	**AE_{ta}**	**AE_t**	**AE_a**	**AE_{ta}**	**AE_t**	**AE_a**	**AE_{ta}**
RMSE	0.637	0.692	0.658	0.575	0.609	0.587	0.637	0.659	0.645
MAE	0.494	0.553	0.516	0.446	0.496	0.464	0.490	0.512	0.498
BIAS	-0.327	-0.337	-0.331	-0.129	-0.101	-0.119	-0.398	-0.384	-0.393
R	-0.187	-0.426	-0.272	-0.191	-0.444	-0.269	-0.259	-0.414	-0.308
Cases	615	374	989	353	189	542	311	169	480

Atmos. Meas. Tech. Discuss., https://doi.org/10.5194/amt-2017-318
Manuscript under review for journal Atmos. Meas. Tech.
Discussion started: 3 November 2017

Atmospheric Measurement Techniques
Discussions

Table 7: Number of coincident cases of AOD_t, AOD_a, AOD_{ta} with BAOD both for DB and for DT algorithms.

Station:	BAOD vs. AOD_t		BAOD vs. AOD_a		BAOD vs. AOD_{ta}	
	DB	**DT**	**DB**	**DT**	**DB**	**DT**
Camagüey	166	171	66	79	232	250
Topes de Collantes	112	138	49	76	161	214
Jovellanos	65	65	35	34	100	99
La Fe	34	66	46	85	80	151
All combined	377	440	196	274	573	714

Table 8: Statistics for the comparison between the single observations BAOD measured at the four actinometrical stations coincident in space and time with the single observation (L2) AOD_t, AOD_a and AOD_{ta}.

	Camagüey, La Fe, Topes de Collantes & Jovellanos					
	BAOD vs. AOD_t		**BAOD vs. AOD_a**		**BAOD vs. AOD_{ta}**	
	DB	**DT**	**DB**	**DT**	**DB**	**DT**
RMSE	0.080	0.087	**0.073**	0.088	0.078	0.088
MAE	0.055	0.063	**0.048**	0.066	0.052	0.064
BIAS	**0.001**	0.027	0.014	0.049	0.005	0.035
R	0.455	0.325	**0.501**	0.417	0.468	0.355
Cases	373	436	191	268	564	704

Table 9: Statistics for the comparison between the single observations time coincident BAOD and AOD_{SP} at all wavelengths measured by the sun photometer at Camagüey. In bold are the best performing value for each statistic.

BAOD vs. $AOD_{SP}(\lambda)$	**1640 nm**	**1020 nm**	**870 nm**	**675 nm**	**500 nm**	**440 nm**	**380 nm**	**340 nm**
RMSE	0.072	0.071	0.057	0.048	**0.044**	0.056	0.081	0.102
MAE	0.062	0.060	0.046	0.037	**0.030**	0.040	0.059	0.076
BIAS	0.060	0.059	0.043	0.032	**-0.002**	-0.022	-0.049	-0.068
R	0.46	0.59	0.65	0.68	**0.69**	0.68	0.67	0.65
Cases	490	877	877	877	**877**	877	877	877

Atmos. Meas. Tech. Discuss., https://doi.org/10.5194/amt-2017-318
Manuscript under review for journal Atmos. Meas. Tech.
Discussion started: 3 November 2017

Atmospheric Measurement Techniques
Discussions
Open Access

Figure and Captions:

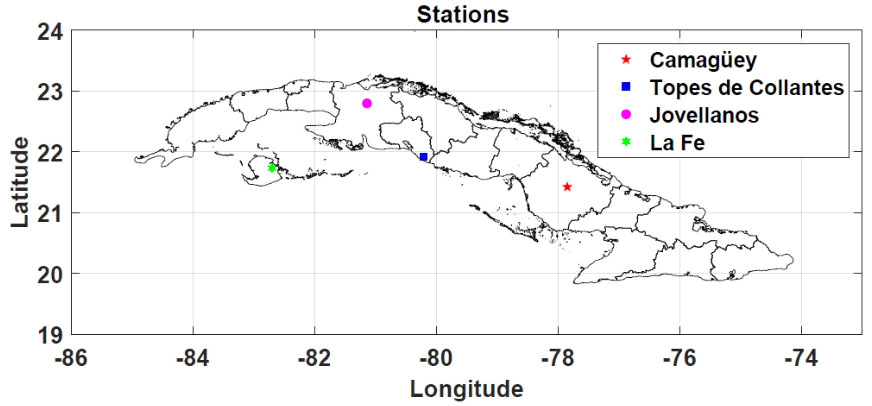

Figure 1: Map of Cuba locating the stations where the sun photometer and the four pyrheliometer measurements are conducted.

Atmos. Meas. Tech. Discuss., https://doi.org/10.5194/amt-2017-318
Manuscript under review for journal Atmos. Meas. Tech.
Discussion started: 3 November 2017

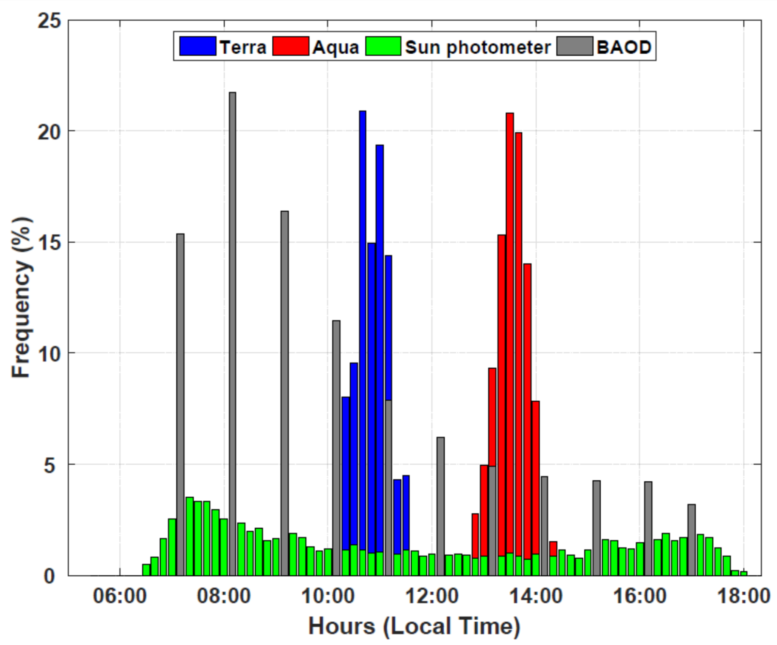

Figure 2: Frequencies of the time of the day (Local Time) the Terra and Aqua (blue and red respectively) overpass Camagüey's sun photometer in a radius of 25 km for the period 2001 to 2015. In green the time frequencies for the Camagüey's sun photometer measurements in the period 2008 to 2014. In addition, the time frequencies for the direct radiation measurements used to calculate the BAOD. The bar width is 10 minutes for Terra, Aqua and the sun photometer and 1 hour for the BAOD.

Atmos. Meas. Tech. Discuss., https://doi.org/10.5194/amt-2017-318
Manuscript under review for journal Atmos. Meas. Tech.
Discussion started: 3 November 2017

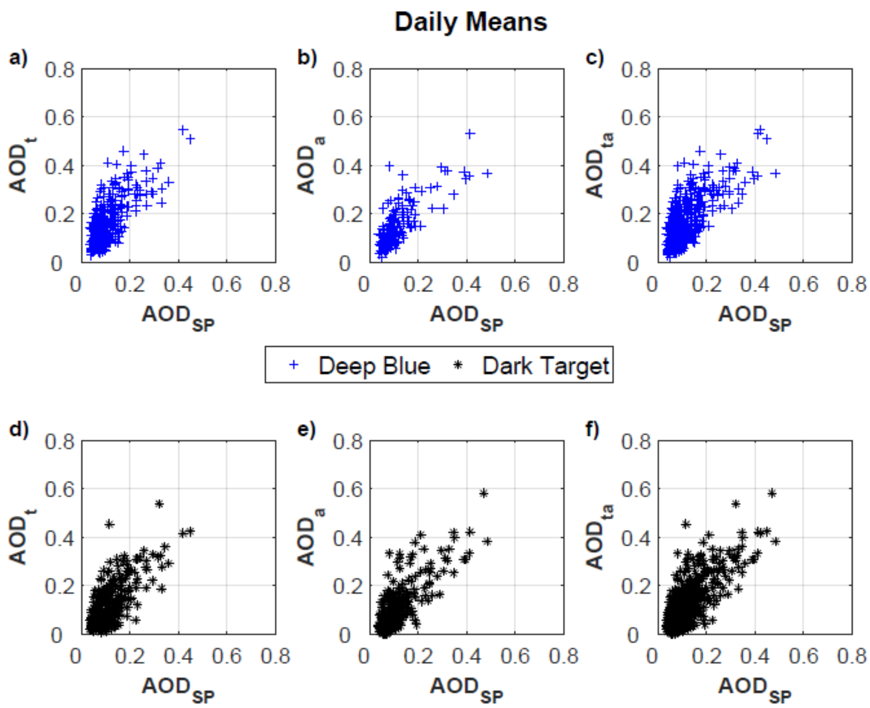

Figure 3: Daily mean scatter plots of the coincident AOD measurements from the sun photometer and Terra and Aqua MODIS instruments for DB and DT algorithms.: a) to c) Daily means of the AOD_{SP} vs AOD_t , AOD_a and AOD_{ta} respectively for DB algorithm; d) to f) Idem for DT algorithm.

Atmos. Meas. Tech. Discuss., https://doi.org/10.5194/amt-2017-318
Manuscript under review for journal Atmos. Meas. Tech.
Discussion started: 3 November 2017

Atmospheric Measurement Techniques
Discussions

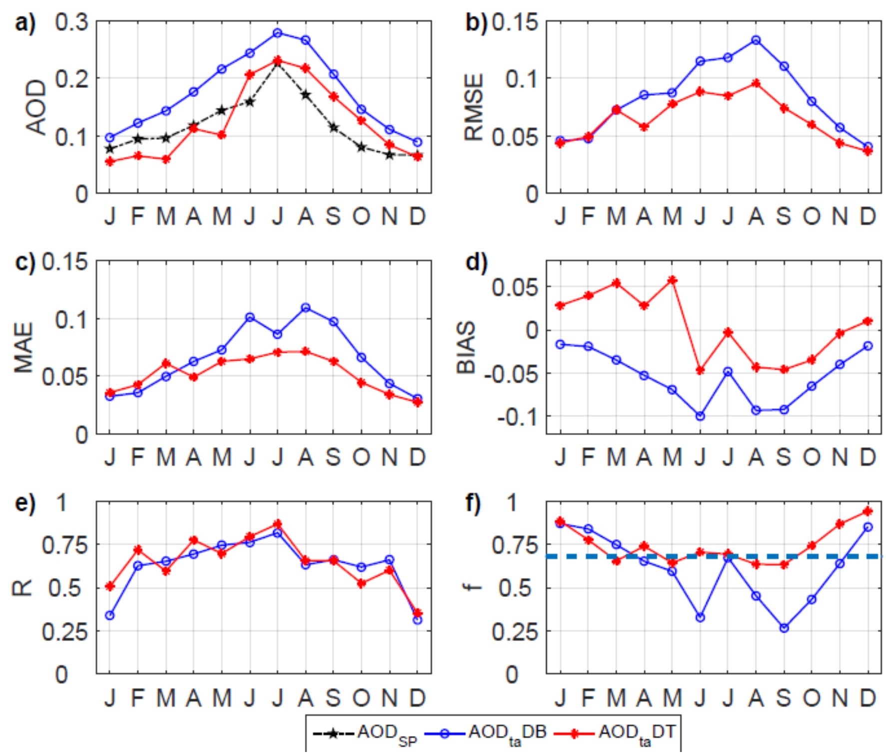

Figure 4: Monthly means and statistics resulting from the comparison between AOD_{SP} and AOD_{ta} for both DB and DT algorithms: a) Monthly means of the AOD_{SP} and AOD_{ta} for both DB and DT algorithms; b) RMSE for the comparison between AOD_{SP} and AOD_{ta} for both DB and DT algorithms; c) Idem for MAE; d) Idem for BIAS; e) Idem for R; f) Idem for f. The blue discontinuous line at f= 68 % represent one standard deviation confidence interval for the EE expression.

Atmos. Meas. Tech. Discuss., https://doi.org/10.5194/amt-2017-318
Manuscript under review for journal Atmos. Meas. Tech.
Discussion started: 3 November 2017

Atmospheric Measurement Techniques
Discussions

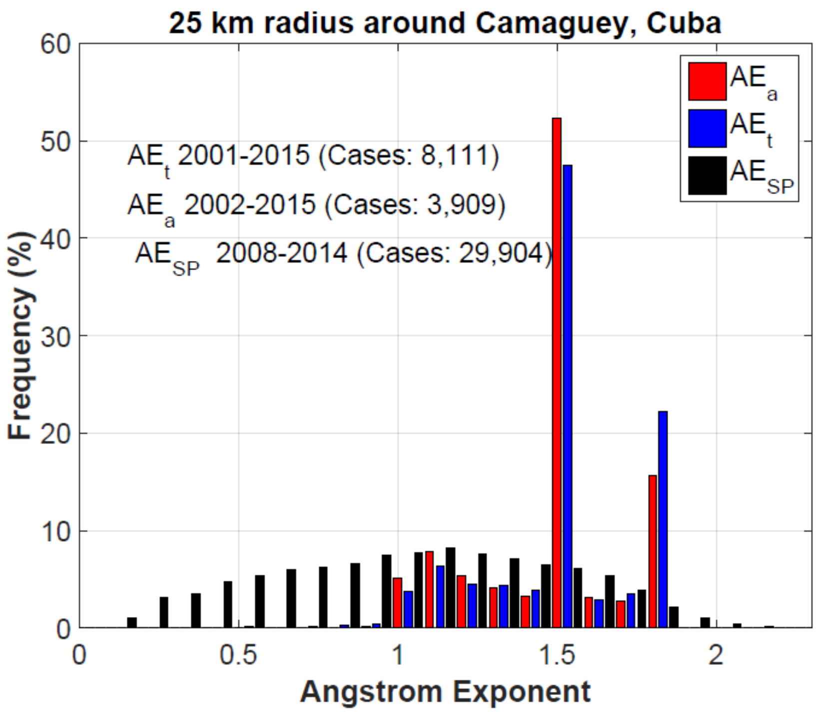

Figure 5: Frequency distribution of the AE_t, AE_a values for all the available values coincident within a 25 km radius around Camagüey. Also included all the AE_{SP} values.

Atmospheric Measurement Techniques
Open Access
Discussions

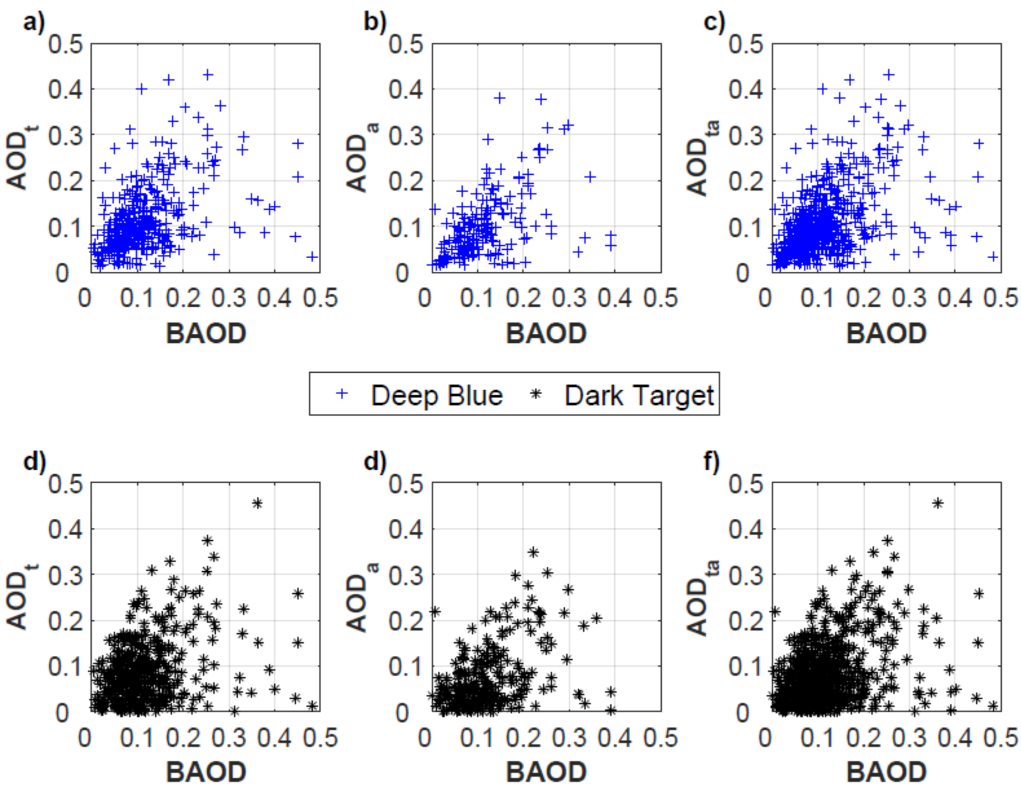

Figure 6: Single observations scatter plots of the coincident BAOD measurements from the pyrheliometer and Terra and Aqua MODIS instruments for DB and DT algorithms.: a) to c) BAOD vs. AOD_t , AOD_a and AOD_{ta} respectively for DB algorithm; d) to f) Idem for DT algorithm.